Iranian Journal of Science & Technology, Transaction B, Engineering, Vol. 33, No. B4, pp 313-326
Printed in The Islamic Republic of Iran, 2009

A NUMERICAL TOOL FOR DESIGN OF DYNAMIC COMPACTION TREATMENT IN DRY AND MOIST SANDS*

A. GHASSEMI[1**], A. PAK[2] AND H. SHAHIR[3]

[1]Dept. of Architecture and Civil Engineering, Islamic Azad University of Qazvin, Qazvin, I. R. of Iran
Email: a_ghassemi@civil.sharif.edu
[2,3]Dept. of Civil Engineering, Sharif University of Technology, Tehran, I. R. of Iran

Abstract– Dynamic compaction (DC) is a popular soil improvement method that is extensively used worldwide. DC treatment design is usually carried out based on past experiences and empirical relations. To establish a rational design approach, all important factors affecting the DC process should be taken into account. In this paper, a finite element code is developed for modeling the impact behavior of dry and moist granular soils. The code is verified with the results of some centrifuge tests. Several analyses were conducted in order to study the effects of energy/momentum per drop, tamper base radius, and number of drops on compaction degree, compacted depth, and extension of the improved zone in the ground. The developed code has considerable capabilities to be used as a tool for designing dynamic compaction treatments.

Keywords– Dynamic compaction, numerical modeling, impact, soil improvement

1. INTRODUCTION

"Dynamic Compaction" is one of the oldest forms of deep soil improvement. The technique consists of repeated dropping of a heavy weight (tamper) in a pre-determined pattern on the weak ground that is going to be densified. The mass of tamper generally ranges from 5 to 30 tons and drop height ranges from 12 to 30 m [1, 2]. Originally, the predominant soil types that are considered for dynamic compaction include ballast fills or natural sandy gravely soils only [3]. But because of the inherent economic advantages involved in the use of DC, a multitude of materials have been improved including hydraulically placed silty sands, clay or silty clay fills, miscellaneous refuse fills, sanitary landfills, mine spoils, rockfills, and collapsible soils [1].

The process of DC design usually includes the following items: selection of tamper weight and drop height, selection of tamper base area, determination of grid spacing, establishing the number of drops per compaction point, and determination of number of phases and their tamping patterns. In usual design approaches, the degree and depth of improvement are assumed to depend on the applied energy per unit volume of soil, and the applied energy per drop, respectively. In this regard, many empirical and semi-empirical correlations between depth of improvement and energy per drop have been established [3-5].

2. REVIEW ON PREVIOUS STUDIES

Various numerical approaches have been used in order to investigate the effect of different factors on DC results and providing a design tool to reduce the cost and time of trial compactions in setting-up DC projects.

The majority of 1-D models consists of a rigid mass impinging on a spring-dashpot system. Generally, 1-D models are not able to determine the lateral extension of improvement in the ground

*Received by the editors April 30, 2007; Accepted April 17, 2009.
**Corresponding author

directly. However, some researchers (e.g. Chow et al. [6]) evaluated the effect of spacing between compaction points using their 1-D model by means of some empirical correlations.

Despite the great advances that have occurred in numerical procedures and computer technology in recent decades, only a few 2-D models have been introduced for simulation of dynamic compaction. Poran & Rodriguez [7] presented one of the earliest 2D models for simulating DC in dry sands using finite element codes DYNA2D [8] and IMPACT [9]. The impact effects assuming large deformation formulation and two different elasto-plastic soil models were analyzed. These soil models were equipped with planar caps to create volumetric plastic strains. The authors did not recommend any hardening function for cap growth, but it may be provided by the user. As the authors remarked, their computed results correlate well when the sand is relatively loose (during the first few impacts), but when densification occurs, the computed results depart substantially from the experimental data.

Pan & Selby [10] used ABAQUS [11] to numerically analyze the response of dry soil to rigid body impacts by a total stress finite element model. In the analyses, non-associated Mohr-Coulomb plasticity model was employed to represent soil behavior.

Based on the valuable findings of Poran & Rodriguez, Gu & Lee [12] described the dry sand behavior under DC process utilizing the finite element program CRISDYN [13]. In this study, an elasto-plastic cap model was used, and assuming that the plastic behavior of the model plays a more important role than its elastic behavior, the elastic soil moduli have not been updated during multiple impacts. Although this numerical model was not able to consider dynamic consolidation in saturated soils, the results are very useful in finding out the mechanisms involved in DC treatment. The effects of drop energy, momentum of the falling tamper, and tamper radius on the depth of improvement were discussed by Lee & Gu [14], who proposed a method for estimating the degree and depth of improvement based on extensive analyses that had been done by the finite element model.

3. NUMERICAL SIMULATION OF DC

Numerical simulation of ground response to dynamic compaction is a complex issue due to the peculiarity of the problem. Some of the important challenges in the numerical modeling of DC are as follows: modeling the effect of falling weight and the appropriate use of contact elements, modeling large deformations/strains, choosing the right values for damping effects, and applying a suitable constitutive model for simulating the soil behavior under impact loads.

First, it is necessary to provide a class of formulations which takes into account all physical phenomena in a DC process. Transferring the falling tamper load to the soil body through the contact surface, wave propagation through soil half space, induced plastic deformations, and gradual changes in the properties of the materials due to densification are among the most important items which must be considered. In this study a developed finite element program 'PISA' was used for analytical purposes. Chan & Morgenstern [15] developed the original version of this multi-purpose geotechnical finite element code (named 'SAGE'). The subsequent versions of this program provided more possibilities for analyzing a large variety of geotechnical problems. Pak [16] increased the program capabilities by amending the formulation for analyzing thermal hydro-mechanical (THM) problems. Shahir [17] added the dynamic analysis ability to the program and used 'PISA' to model liquefaction phenomenon in loose saturated sand deposits. Liquefaction phenomenon has been simulated using different methods by other researchers too [18]. Ghassemi [19] further developed the program for simulation of dynamic compaction. He added special cap models to the code and investigated the effects of different constitutive laws in the numerical modeling of DC.

a) Wave propagation

In the finite element program 'PISA', the ability for fully coupled dynamic analyses has been provided. So governing field equations, namely equilibrium (or momentum balance) for the soil-fluid

mixture and momentum balance for the fluid phase can be solved simultaneously. The spatial discretized form of these equations in the simplified U-P form is as follows [20]:

$$M\ddot{U} + C\dot{U} + \int_V B^T \sigma' dV - QP - f^{(1)} = 0 \tag{1}$$

$$Q^T \dot{U} + HP + S\dot{P} - f^{(2)} = 0 \tag{2}$$

where M is the mass matrix, C the viscous damping matrix, U the solid displacement vector, B the strain-displacement matrix, σ' the effective stress tensor (determined by soil constitutive model which will be discussed later), Q the discrete gradient operator coupling the motion and the flow equations, P the pore pressure, S the compressibility matrix, and H the permeability matrix. The vectors $f^{(1)}$ and $f^{(2)}$ include body forces and fluid flux, respectively. By solving the above system of equations, soil deformation (U) and generated pore pressure (P) can be determined at any desired point in the soil mass.

In a two-phase saturated system, pore water pressure and deformation of solid particles in the soil are inter-related and a fully coupled analysis of the system should be carried out. But when impact loads are applied to dry soils, since no pore pressure exists, the terms containing P are eliminated and the above two equations are reduced to the familiar equation of equilibrium in dynamic form:

$$M\ddot{U} + C\dot{U} + \int_V B^T \sigma' dV = f \tag{3}$$

b) Modeling impact

In the finite element context, impacts are modeled in two main ways:

1) By applying acceleration records from experimental data as a load history to the continuum composed by the soil and tamper.
2) By considering initial velocity for tamper which can be determined from the free fall equation.

The second method has been used successfully by Poran & Rodriguez [7], Pan & Selby [10] and Pak et al. [21]. Because of its applicability, the second method is employed in the present study.

c) Soil constitutive model

Most of the early DC models were introduced by adopting elastic behavior for soil (e.g. Chow et al. [22]). It is obvious that for modeling permanent deformations observed in the compaction process, applying inelastic constitutive laws is inevitable. Furthermore, classic perfect plastic models are not of interest, since there is no possibility of compression yield in such models, despite the fact that part of the soil mass may yield especially under high compressive stresses.

Cap models seem to be useful, particularly for modeling soil behavior under impact loads [7, 12]. The modern series of cap models was introduced by Dimaggio & Sandler [23]. These models utilize the classical plasticity approach, so the yield surface is their defining characteristic. The yield surface is composed of a shear failure envelope, a movable cap and a tension cut off.

Cap models have been successfully used for simulation of DC in granular soils by Thilakasiri et al. [24], Gu & Lee [12] and Pak et al. [21]. Herein the cap model with a single shear yield surface is used for the analyses. The expressions for shear failure surface (F_1) and cap locus (F_2) are given by:

$$F_1 = \sqrt{J_{2D}} - \alpha J_1 - \kappa = 0 \tag{4}$$

$$F_2 = (J_1 - l)^2 + R^2 J_{2D} - (x - l)^2 = 0 \tag{5}$$

α and κ are material parameters that are functions of internal friction angle (φ) and cohesion (c). R is the ratio of the major axis to minor axis of the cap ellipse. The values of R depend on the shape and size of the yield cap [25].

l is the J_1 value of the intersection point of shear failure locus and the cap, and x is the hardening parameter which depends on plastic volumetric strain (ε_V^P) as follows:

$$x = \frac{-1}{D} Ln(1 - \frac{\varepsilon_V^P}{W}) + x_0 \tag{6}$$

W, D and x_0 are also material parameters. W and D can be obtained from hydrostatic compression test [25]. The smaller values of W and D indicate that the soil shows higher compressibility.

d) Reassignment of elastic parameters

The relative density of the soil mass under impact loads increases significantly, especially in the vicinity of the contact surface. It is crucial to consider the variation of material properties during the process of numerical simulation of DC. In some published numerical models, the improvement of material properties has been assumed at the end of each impact and at the beginning of the next one. For example, Chow et al. [26] used a series of empirical correlations to update the elastic modulus of the soil column before applying the subsequent impact loads.

During the DC process, high energy stress waves propagate through the ground. So each element of soil experiences a high pulse of confining pressure for a very short period of time. This would cause a temporary change of soil properties, having considerable effects on compaction results. Gu & Lee [12] took into account a simple linear relationship between mean effective stress (P') and the bulk modulus of soil mass (K). Although such method can model the dependency of elastic modulus on the stress state; it is not able to simulate the permanent increase of soil stiffness after each blow based on the increase in relative density of the soil under impact.

From the above discussion, it seems logical to apply a relationship which involves the effects of the variation of the stress state and the relative density on the elastic properties. On the other hand, the relative density of compacted soil changes gradually during the impact pulse and it is more realistic to apply a continuous function instead of a stepwise increase of relative density after each impact. In this study, the following equations have been considered:

$$K = K_r P_a (\frac{P'}{P_a})^{0.5} \tag{7}$$

$$K_r = \beta \exp(\gamma D_r) \tag{8}$$

where K is the bulk modulus, P' is the mean effective stress, D_r is the relative density, Pa is the atmospheric pressure, and β and γ are soil constants. These constants relate the soil bulk modulus to changes in P' and D_r. Equation (7) has been proposed for sandy soils by Poran and Rodriguez [7]. These investigators, based on the results of a number of laboratory tests conducted on sands, have suggested β and γ to be equal to 120.0 and 0.0134, respectively, to match the values predicted by this empirical relation with laboratory results.

e) Other aspects of the finite element model

The equation of equilibrium in dynamic form can be solved in two or three dimensions. However, since the geometry and loading configuration are symmetric around the axis of the falling tamper (load centerline), two-dimensional axisymmetric simulation usually yields satisfactory results.

Descritized domain should be considered large enough so that the reflection of stress waves from the boundaries is limited. In this case, the critical part of analysis occurs in the first passage of the outgoing semi-spherical wave front and it is usually unnecessary to use special boundary elements like infinite elements [10]. The suitable dimension of the model can be selected after some trial and error.

The element size, especially at the vicinity of the impact, should be small to represent the intense stress and deformation gradients. So the element size and time step are two related parameters which must be considered together. Hallquist [27] indicated that the critical time step size is related to the time taken to propagate an elastic wave across the shortest dimension of the element. It must be realized that not only too large element dimensions cause filtering high frequency waves, but also very small element dimensions may render numerical instability. Small elements require considerable computational resources as well [28].

In the numerical modeling of DC, the most important factor affecting the size of the time step is the approach of applying the impact load. In the analyses in which acceleration (or stress) record is used as loading, usually a larger order of time step is sufficient; but when initial velocity is applied, to induce a realistic load–time history, a much smaller time step is required. For example, Pan & Selby [10] used Δt of 5×10^{-3} seconds for the analyses with force-time loading approach and Δt of 1×10^{-6} s for the analyses with a rigid body impact loading (initial velocity) approach. Herein, the time step of 5×10^{-5} s is used according to the results of the sensitivity analyses [19].

The duration of an impact load step depends on the imposed drop energy. Each step of the finite element analysis should continue until the tamper oscillations tend to zero. After contact, the acceleration of the tamper decreases rapidly until the tamper stops and then starts to move up. Consequently, the tamper elements pull the soil elements up till the sign of the velocity changes again. Despite the occurrence of this unreal tension in the soil column, numerical solutions in the present study have shown that its effects are not critical. The use of special contact elements may be useful to decrease this unfavorable effect.

When impact loads are applied, large strains and deformations usually occur in the soil near the tamper. In this study, large deformation is taken into account using mesh-update procedure. In this procedure, the nodal coordinates of the mesh are updated at the end of each loading, using the nodal displacements calculated in this load step. However, large strains are not included in this version of the numerical model.

Another important aspect of dynamic analysis of DC is attenuation (both numerical and material). In PISA, the Newmark integration parameters control the numerical attenuation, whereas for material attenuation, the standard Rayleigh damping equation has been applied. The Rayleigh damping constitutes convenient measures that lump the effects of the mass and stiffness matrices of the elements as proposed by Idriss et al. [29] for a variable damping solution. The damping matrix for the entire system would be obtained by assemblage of the submatrices of the elements.

4. VERIFICATION OF THE MODEL

In order to verify the developed numerical tool for dry soils, comparisons were made with Oshima & Takada's [30] centrifuge tests conducted on nearly dry sand under the centrifugal acceleration of 100g. The model material was a sandy soil passing the 2 mm sieve with a fine fraction of 6%. The model ground was compacted to the initial density of 35% with a water content of 4%.

The 2-D axisymetric finite element mesh shown in Fig. 1 was used for modeling the tests in prototype dimensions. The parameters for the cap model were chosen based on Gu & Lee's [12] numerical analyses

in which they studied a similar sandy soil. The initial cap parameter (x_0) was selected based on gravity analysis, i.e. x_0 is different for each row of elements in the mesh due to variation of in-situ stress in depth. Furthermore, as the elastic parameters of the soil were unknown, the suggested values of β and γ (Eq. (8)) by Poran & Rodriguez [7] were used in this study. The applied constitutive parameters of the modelled soil are presented in Table 1.

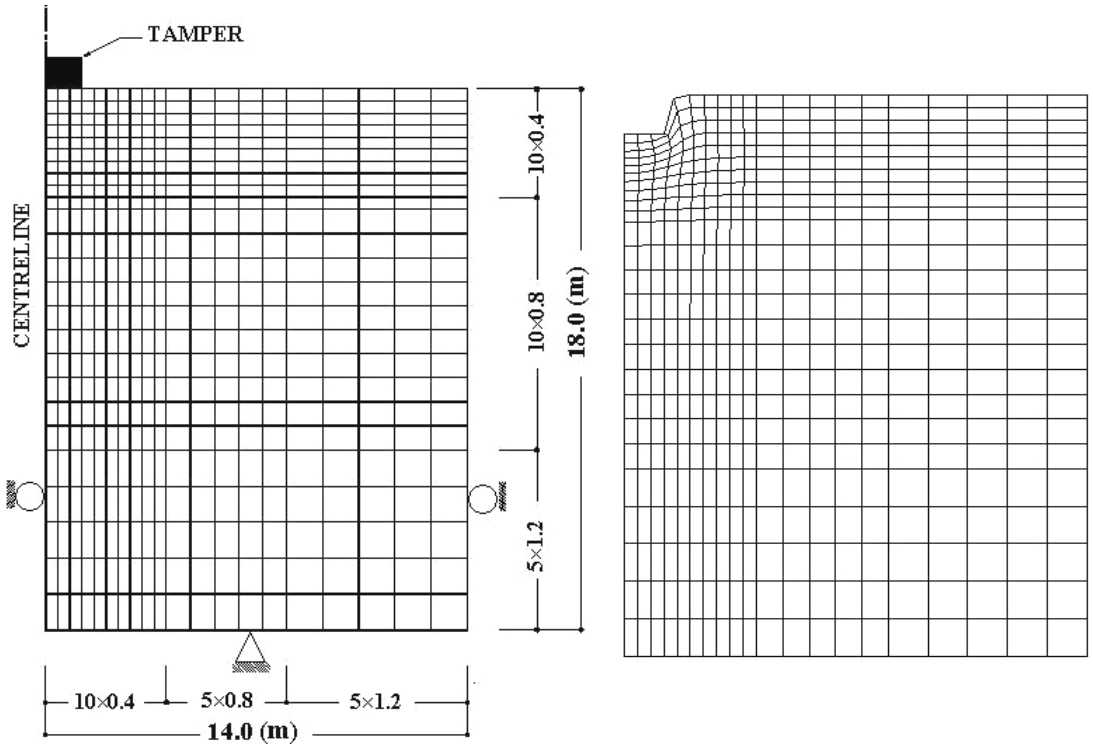

(a) (b)

Fig. 1. a) Finite element mesh and boundary conditions, b) Deformed mesh after a number of impacts

Table 1. Soil parameters in the analyses [7, 12]

Elastic			Plastic				
β	γ	υ	α	κ	R	W	D (m^2/kN)
120	0.0134	0.25	0.23	0.0	4.33	0.4	.00018

In the course of simulation of the centrifuge tests mentioned above, numerous analyses were done by the developed software with different drop energies, momentum, number of drops and tamper base radius. The results of an example illustrating relative density increase for a 400 t.m energy per drop (W=20t and H=20m) is shown in Fig. 2. In this figure, the results of the centrifuge tests and numerical analyses in the form of contour lines of relative density increase (ΔDr=10, 20 and, 40%) are presented. The contour lines of relative density increase after the 10th drop is close to the recorded data in depth; for lateral extension there is some difference (about 7%) between the numerical and experimental results. On the other hand, after the 20th drop, the depth of the predicted contour lines were smaller (about 5%) than those observed by Oshima & Takada, but the extension of the contour lines is better matched with the test results in comparison with the 10th impact.

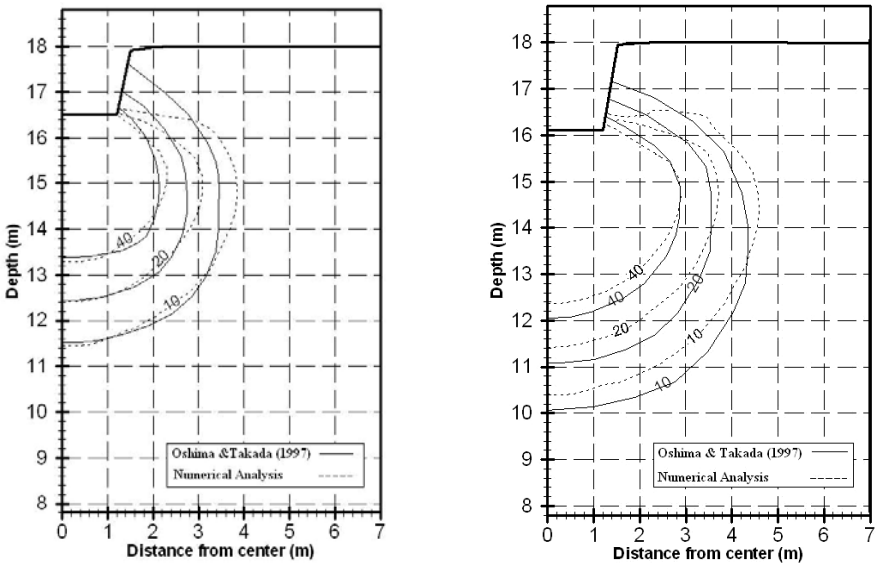

(a) (b)

Fig. 2. Contour lines of 10, 20 and 40% increase in Dr after, a) 10 drops, b) 20 drops

Oshima & Takada [30] defined the compacted area in terms of depth (Z) and radius (R) of the bulb shaped area of relative density increase as shown in Fig. 3. For example, Z10 and R10 designate the depth and radius of the bulb corresponding to the relative density increase of 10%, respectively. In the following, these symbols are used with the same definitions for easy comparison between the numerical and experimental results.

Oshima & Takada [30] showed that depth (Z) and radius (R) of the compacted area have almost linear relations with the logarithm of the total momentum of drops during DC. Their proposed relations have been plotted in Fig. 4. To compare with these relations, numerical results of this study were added to the chart. As can be seen in Fig. 4, the numerical results are well in agreement with the trends of the proposed lines, but as the total momentum increases, the deviation of the numerical results from the experimental lines increases. To explain the reason, investigation should be focused on soil hardening behavior due to the high energy (or momentum) of dynamic compaction.

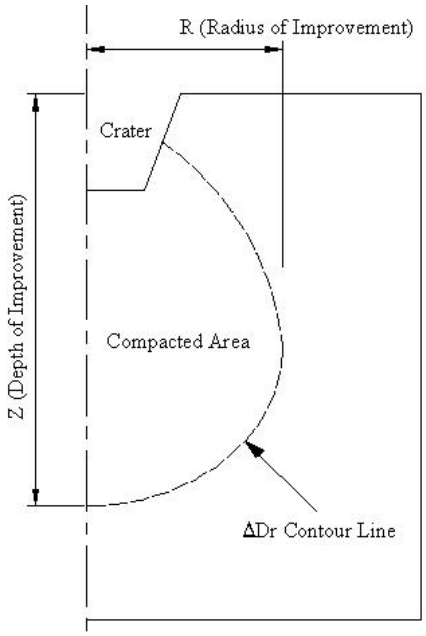

Fig. 3. Definition of compacted area

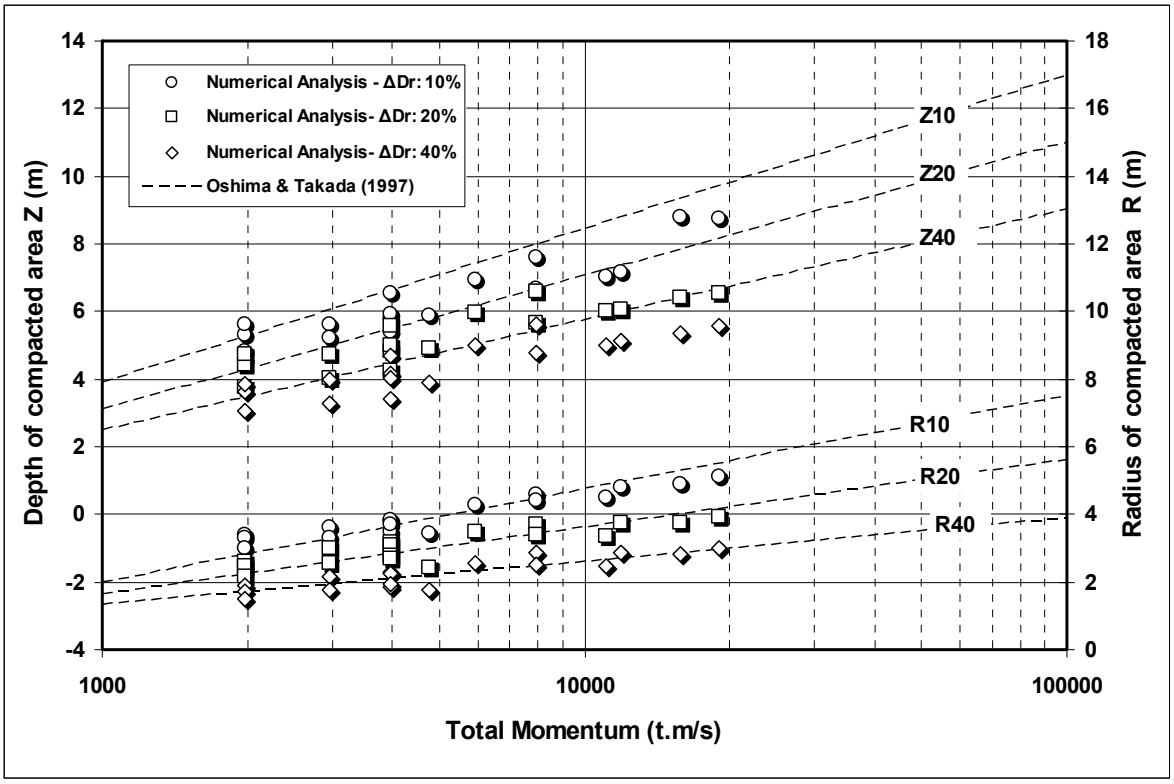

Fig. 4. Relation between compacted area and total momentum

5. USING THE DEVELOPED NUMERICAL TOOL FOR DC DESIGN

Applied energy per drop (WH) is the most important factor affecting the depth of improvement in a given ground condition. Many studies have been done and various relations are available for predicting the maximum depth of improvement as a function of energy per drop [3-5]. Among these relations, Menard formula has been the most popular empirical expression between DC practitioners:

$$DI = n\sqrt{WH} \tag{9}$$

where DI is the depth of improvement, W is the weight of tamper (in tons), H is drop height (in meters) and n is an empirical coefficient including all the remaining factors affecting DC treatment. Mayne et al. [1] indicate that n may vary between 0.3 and 0.8. Most of the available guidelines in the literature present values of n according to ground conditions.

It is clear that simple relations such as Eq. (9) cannot consider all important issues such as number of drops, shape of tamper, ground water level, falling system, etc. Furthermore, in Menard's formula a clear definition for depth of improvement has not been provided (in terms of the improvement of relative density or other relevant parameters).

In this section, the effects of two important equipment-related factors in DC design which are not considered in the Menard relation directly (drop number and radius of tamper), are studied utilizing the developed modeling tool.

a) Multiple drops

The effects of multiple drops on crater depth and also dimensions of the compacted zone will be investigated here.

Crater depth: since the falling weight energy is applied on a pre-determined grid, the most obvious manifestation of the DC process is the relatively large craters induced in each compaction point. Crater depth is a useful item in quality control of DC treatment. The increase in cumulative crater depth during multiple impacts is a simple sign of the continuing improvement process. Mayne et al. [1] collected the field measurements of over 120 sites to study the response of the ground to DC. They showed that when the crater depth measurements are normalized with respect to the square root of energy per drop, the data fall within a rather narrow band. On the other hand, there are some observations that crater depth has a linear relation with the square root of drop counts [31, 32]. The relationship between these values is depicted in Fig. 5. The results of the numerical model are also plotted in Fig. 5 to show the relationship between the normalized crater depths with the square root of drop number. The computed results were compared with those analyzed by Mayne et al. [1] for 300-400 t.m energy per drop from a number of DC sites. The linear trends can be seen in both the numerical and the experimental data. The interesting point is the complete overlapping of the lines for different energies in the numerical results which shows a good agreement with the field measurements as well. The crater depth becomes larger than the actual values for larger N. This discrepancy may be attributed to neglecting the large strains in the formulation of the model. Linear variation obtained from numerical simulations and the relatively narrow band obtained from field measurements both indicate that the normalized crater depth is only a function of N. In other words, the soil type and tamper size do not contribute to the results.

Compacted area: As the source of energy in DC is located at the ground surface, it is reasonable to assume a threshold energy in which the application of higher energies would no longer be effective to reach deeper depths in the ground. This fact is not compatible with the linear relation in the Menard formula. To study this idea, results of the numerical analyses are presented in Fig. 6. A minimum increase of 5% in relative density at depth (Z5) is chosen to delineate the improved zone. Considering this figure, it seems that application of the Menard formula ($n = 0.5$) for higher impact energies may lead to overestimation of the improvement depth in sandy soils. In this figure, variation of Z5 with the square root of energy per drop is also shown. It can be seen that the presence of threshold energy in numerical results is in agreement with that suggested by Scolombe [5] (Fig. 6).

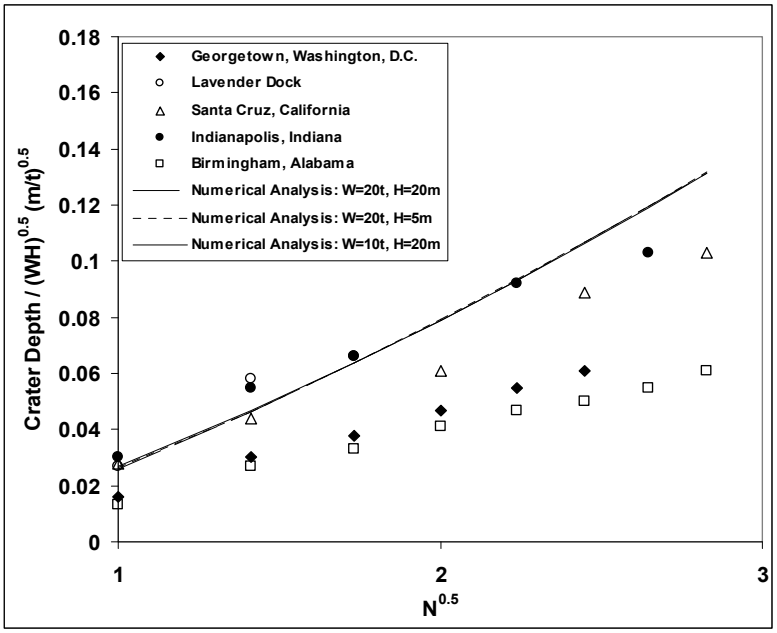

Fig. 5. Relation between normalized crater depth and $\sqrt{N}$

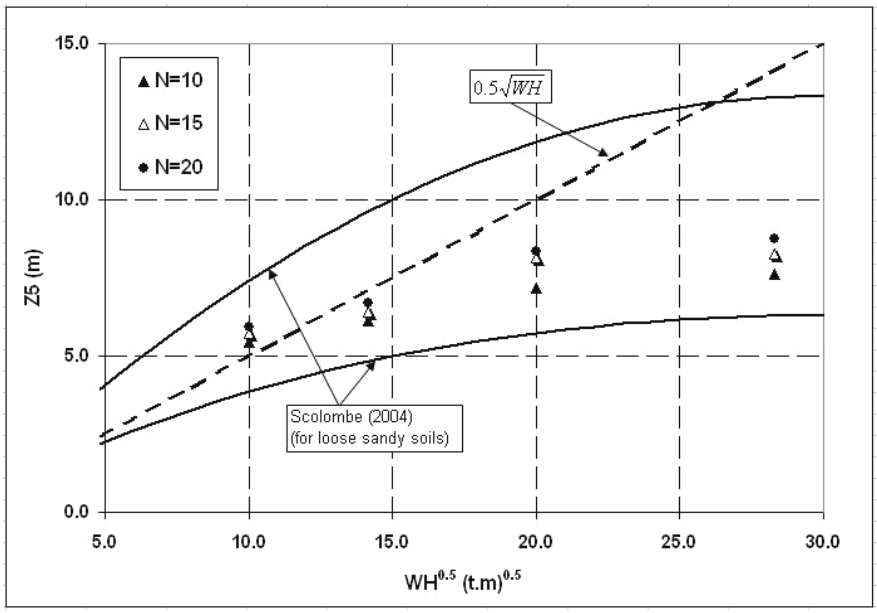

Fig. 6. Relation between depth of improvement and square root of applied energy

Additionally, the computed data indicate that the soil underwent no significant further compaction after about 15 blows (Fig. 7). The concept of limiting drop number corresponding to a threshold state of energy is already well known [5]. The limiting drop number is basically dependent on the soil type under treatment.

Scolombe [5] described the depth of improvement as a depth in which little or no further improvement in the ground is possible. Considering this definition and assuming the presence of a limiting drop number (N_{th}), it is important to note that the Menard formula predicts the maximum achievable depth of improvement after blowing equal or more than limiting drop number. Hence, it is practically useful to find the interim depth of improvement (Z_i), when insufficient drops ($N_i < N_{th}$) are applied. Figure 8 shows this concept using two dimensionless variables α_Z and α_N being defined as:

$$\alpha_Z = \frac{Z_i}{Z_{\max}} \quad , \quad \alpha_N = \frac{N_i}{N_{th}}$$

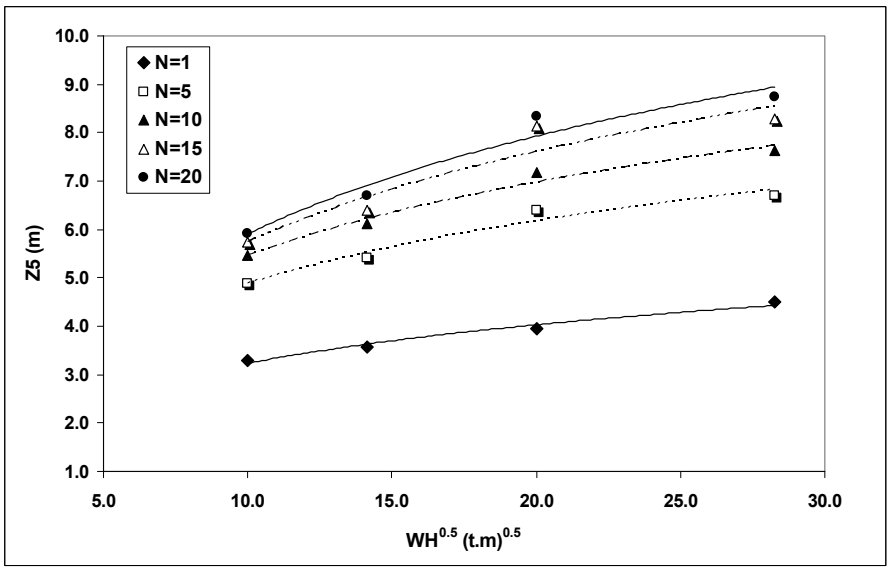

Fig. 7. Limiting drop number

These variables had been used by Lee & Gu [14] to present a relation which gives interim depth of improvement when Z_{max} is known. In Fig. 8, Oshima & Takada's [19] and Lee & Gu's (2004) [12] data, as well as the results of the present numerical analyses are shown. Lee & Gu [14] reported that a well-fitted trendline through the data points is a half-circular curve ($\alpha_Z = \sqrt{1-(1-\alpha_N)^2}$). Here, based on the obtained numerical results, a half-ellipsoidal curve is proposed, defined by:

$$\alpha_Z = \sqrt{1-(1-\alpha_N)^2/1.2} \tag{10}$$

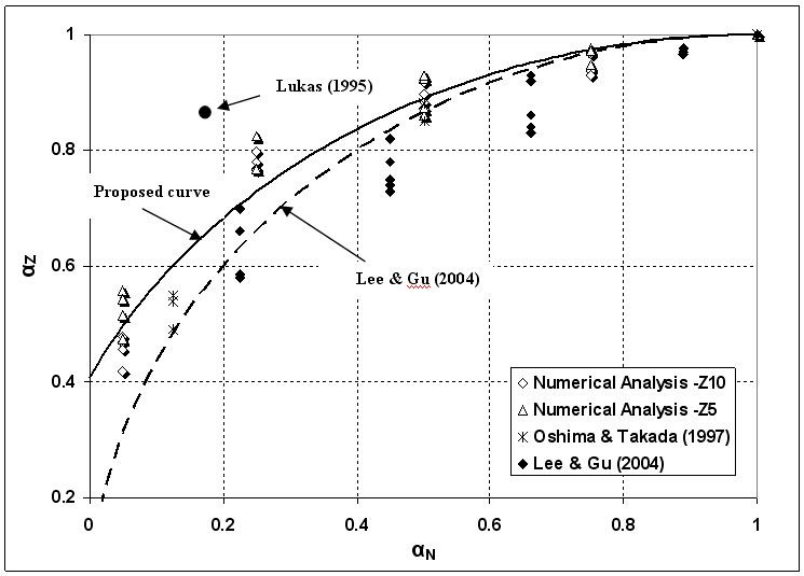

Fig. 8. Interim depth of improvement

This curve presents a better fit to both the experimental and the numerical results. Thus by assuming N_{th} (equal to 15 drops) and Z_{max} (from Eq. (9)), one can estimate the interim depth of improvement easily by using the above equations. For example, the graph shows that after blowing 4 drops, the attainable percent of the maximum depth of improvement is 60% and 68% by using Lee & Gu's equation and Eq. (10), respectively.

Lukas [2] implies that in the case of sandy deposits, approximately 90% of maximum depth of improvement is achieved after 2 to 4 drops. The proposed curve seems to provide more reliable results compared to Lee & Gu's curve.

b) Tamper base area

Compacted area: It has been found by experience that the desired depth of improvement is achieved with neither the smallest nor the largest radius of tamper. Lukas [2] reported that most tampers have a flat bottom with a contact pressure (=W/A) on the order of 40 to 75 kPa. In fact, if the contact pressure is significantly less than the lower bound, the energy is distributed over a too wide area and a hard surface layer develops without considerable depth of improvement. Contact pressures significantly higher than the typical values could result in tamper plugging into the ground without further improvement. These findings indicate that there is an optimum radius tamper and its value depends on the weight of the tamper.

There are a few numerical investigations in which the effects of the tamper base area on the depth of the improvement zone have been studied. Yong [33] used a 1-D DC model and his results showed that the depth of improvement decreases with the increase of the tamper base area. Lee & Gu [14] and Ghassemi [19] reported a contradictory result which showed that there is an intermediate radius giving the maximum depth of improvement.

Figure 9 shows the variations of depth and radius of compacted area with tamper base radius. In the presented cases in Fig. 9, one drop has been applied with a drop height of 20 m. As Fig. 9a shows, variation of the improvement depth with tamper radius demonstrates a group of curves having a peak. The peak value in each case shows the optimum tamper radius to be used. Also, it can be seen from Fig. 9b that similar to the relation of crater depth and radius of tamper, a linear relation between radius of improvement zone and radius of tamper base can be established. It should be noted that dynamic compaction with a tamper diameter less than 1.5 m is not usual in practice. As can be seen in the figure, the numerical results justify this, since the depth of improvement for small radia is too low.

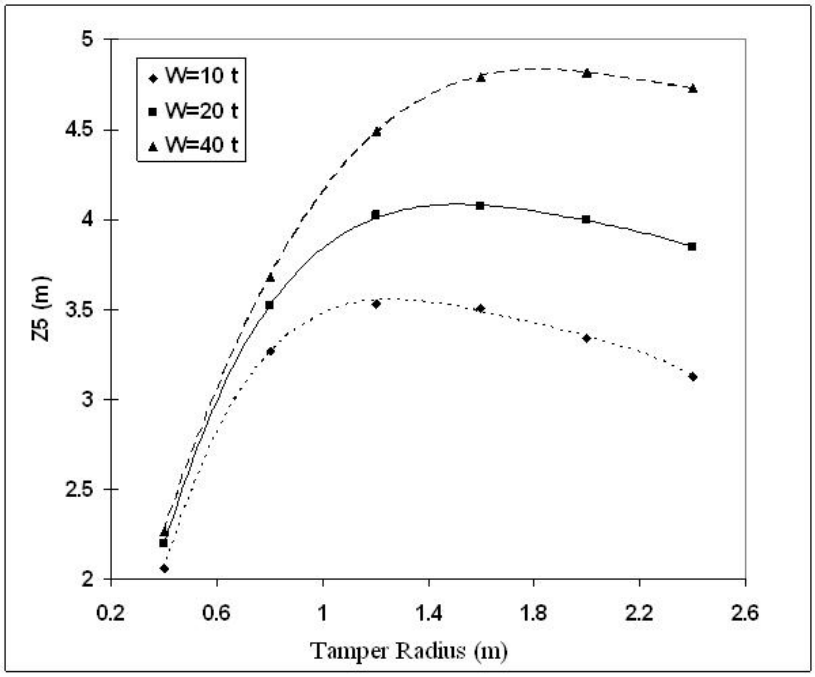

Fig. 9. a) Relation between tamper radius and depth of improvement

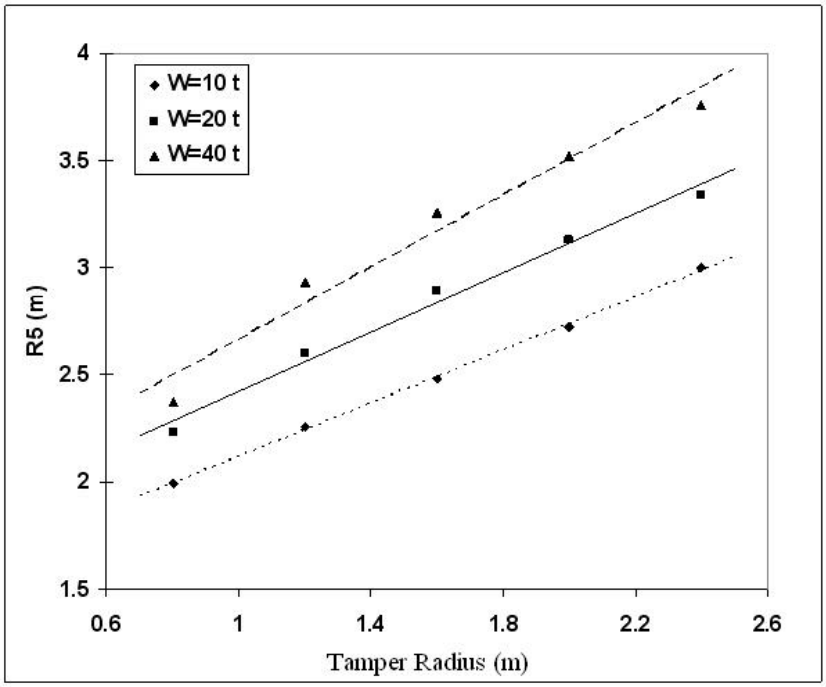

Fig. 9. b) Relation between tamper radius and radius of improvement

6. CONCLUDING REMARKS

A finite element code is developed which is able to simulate the DC treatment in dry and moist soils. The impact of tamper on the ground surface was modelled by applying initial velocity to tamper elements. To consider compression yield and plastic hardening of soils under impact loads, a cap model with single shear yield surface and elliptical cap locus was used. In addition to plastic hardening, the temporary effects of propagation of high energy stress waves through the ground on one hand, and permanent effects of relative density change on the elastic properties of soil on the other, play important roles on the compaction results. By adopting a simple relation in the code, elastic parameters of the soil can be updated based on mean effective stress and relative density.

Several numerical simulations have been carried out using the developed code to examine the effects of different drop energies, momentum, number of drops, and tamper base radii. The results indicate that the numerical model can well predict the depth and radius of the compacted zone. However, as the total momentum increases, the deviation of the numerical results from the recorded values during centrifuge tests gradually increases.

Numerical results indicate that the effects of multiple drops on the crater depth and growth of the compacted zone can be determined by the model. One of the interesting points is the linear trend between the normalized crater depth (crater depth/$\sqrt{WH}$) with the square root of drop number. Additionally, the presented results confirm the existence of a limiting drop number (applying more than that cannot increase the depth of improvement) which is empirically well known.

It is a common practice to use the Menard relation for estimating the depth of improvement in DC treatments. However, such a formula is only able to give the maximum (final) depth of improvement. By using the developed numerical tool, a helpful graph was presented which can be used to predict the interim depths of improvement before the limiting drop number is applied. The effects of tamper radius on the crater depth and the compacted area were also investigated in this study. The results pertaining to the variation of improvement depth with tamper radius demonstrate a group of curves which can be used for selecting the optimum tamper radius in DC treatments.

REFERENCES

1. Mayne, P. W., Jones, J. S. & Dumas, J. C. (1984). Ground response to dynamic compaction. *ASCE 110*, GT6, pp. 757-773.
2. Lukas, R. G. (1995). Geotechnical Engineering Circular No.1-Dynamic compaction. *FHWA-SA-95-037*.
3. Menard, L. & Broise, Y. (1975). Theorical and practical aspects of dynamic consolidation. *Geotechnique*, Vol. 25, No. 1, pp. 3-16.
4. Luongo, V. (1992). Dynamic compaction. Predicting depth of improvement. *GSP*, Vol. 2, No. 30, pp. 927-939.
5. Scolombe, B. C. (2004). Dynamic compaction. *Ground improvement*, Moseley, M.P., Ed., pp. 93-118.
6. Chow, Y. K., Yong, D. M, Yong, K. Y. & Lee, S. L. (1994). Dynamic compaction of loose granular soils: effect of print spacing. *J. Geotech. Eng.*, Vol. 120, No. 7, pp. 1115–1133.
7. Poran, C. J. & Rodriguez, J. (1992). A finite element analysis of impact behavior of sand. *Soils and Foundations*, Vol. 32, No. 4, pp. 68-80.
8. Hallquist, J. O. (1988). User's manual for DYNA2D- An explicit two dimensional hydrodynamic finite element code with interactive rezoning and graphical display. UCID-18756, Rev.3.
9. Rodriguez, J. A. (1990). Finite element analysis of impact in sand. *Ms Thesis*, Uni. of North California.
10. Pan, J. L. & Selby, A. R. (2002). Simulation of dynamic compaction of loose granular soils. *Adv. in Eng. Software*, Vol. 33, pp. 631-640.
11. Hibbit, Karlsson and Sorensen Inc. (1998). ABAQUS 5.8.

12. Gu, Q. & Lee, F. H. (2002). Ground response to dynamic compaction. *Geotechnique*, Vol. 52, No. 7, pp. 481-493.
13. Goh, S. H. (1995). Propagation and attenuation of ground shock in dry soils. *Ph.D. Thesis*, National University of Singapoore
14. Lee, F. H. & Gu, Q. (2004). Method for estimating dynamic compaction effect on sand. *J. of Geotech. Geoenvir. Eng.*, Vol. 130, No. 2, pp. 139-152
15. Chan, D. & Morgenstern, N. R. (1988). SAGE: A finite element program for stress analysis in geotechnical engineering, program user manual. Geotechnical Group, the University of Ablerta.
16. Pak, A. (1997). Numerical modeling of hydraulic fracturing. *Ph.D. Thesis*, Department of Civil and Environmental Eng., University of Alberta.
17. Shahir, H. (2002). Dynamic analysis of saturated porous medium to numerical modeling of liquefaction. *M.Sc. Thesis*, Sharif University of Technology.
18. Sadrnejad, S. A. (2007). A general multi-plane model for post-liquefaction of sand. *Iranian Journal of Science and Technology, Transaction B, Engineering*, Vol. 31, No. B2, pp. 123-141.
19. Ghassemi, A. (2004). Numerical modeling of dynamic compaction of dry and saturated soils. *M.Sc. Thesis*, Sharif University of Technology.
20. Zienkiewicz, O. C., Chan, A. H. C., Pastor, M., Schrefler, B. A. & Shiomi, T. (1999) Computational geomechanics with special reference to earthquake engineering. John Wiley.
21. Pak, A., Shahir, H. & Ghassemi, A. (2005). Behavior of dry and saturated soils under impact load during dynamic compaction. *Proc.16th ICSMGE*, Osaka.
22. Chow, Y. K., Yang, D. M., Yang, K. Y. & Lee, S. L. (1990). Monitoring of dynamic compaction by deceleration measurements. *Comp. and Geotech.*, Vol. 10, No. 3, pp. 189-209.
23. Dimaggio, F. L. & Sandler, I. S. (1971). Material Model for Granular Soils. *J. Eng. Mech. Div.*, ASCE, Vol. 97, EM3.
24. Thilakasiri, H. S., Gunaratne, M., Mullins, G., Stinnette, P. & Kuo, C. (2001). Implementation aid for dynamic replacement of organic soils with sand. *J. Geotech. Geoenv. Eng.*, Vol. 127, No. 1.
25. Desai, C. S. & Siriwardane, H. J. (1984). *Constitutive laws for engineering materials with emphasis on geologic materials*. Prentice-Hall Inc. NJ 07632.
26. Chow, Y. K., Yong, D. M. & Lee, S. L. (1992). Dynamic compaction analysis. *J. Geotech. Engng*, Vol. 118, No. 8, pp. 1141–1157.
27. Hallquist, J. O. (1983). Theoretical manual for DYNA3D. Lawrence Livermore National Laboratory, University of California.
28. Zerwer, A., Cascante, G. & Hutchinson, J. (2001). Parameters estimation in finite element simulations of Rayleigh waves. *J. Geotech. Geoenv. Eng.*, Vol. 128**,** No. 3, pp. 250-261.
29. Idriss, I. M., Seed, H. B. & Serft, N. (1974). Seismic response by variable damping finite element. *J. Geotech. Eng.*, Vol. 100, No. GT1, pp. 1-13.
30. Oshima, A. & Takada, N. (1997). Relation between compacted area and ram momentum by heavy tamping. *Proc. 14th ICSMFE*, Vol. 3, pp. 1641–1644.
31. Mikasa, M., Takada, N., Ikeda, M. & Takeuchi, I. (1988). Centrifuge model test of dynamic consolidation. *Proc. Int. Conf. Geotech Centrifuge Modeling*, pp. 185-192.
32. Takada, N. & Oshima, A. (1994). Comparison between field and centrifuge model test of heavy tamping. *Proc. Centrifuge 94,* Singapore, pp. 337–342.
33. Yong, D. M. (1993). Ground improvement by dynamic compaction. *PhD Thesis*, National University of Singapore.